White Rose Research Online

eprints@whiterose.ac.uk
https://eprints.whiterose.ac.uk
Universities of Leeds, Sheffield and York

Deposited via The University of Sheffield.

White Rose Research Online URL for this paper:
https://eprints.whiterose.ac.uk/id/eprint/148810/

Version: Accepted Version

Article:
Rodríguez-Ochoa, R., Olarieta, J.R., Santana, A. et al. (2019) Relict periglacial soils on Quaternary terraces in the central Ebro Basin (NE Spain). Permafrost and Periglacial Processes, 30 (4). pp. 364-373. ISSN: 1045-6740

https://doi.org/10.1002/ppp.2005

This is the peer reviewed version of the following article: Rodríguez-Ochoa, R, Olarieta, JR, Santana, A, et al. Relict periglacial soils on Quaternary terraces in the Central Ebro Basin (NE Spain). Permafrost and Periglac Process. 2019; 1– 10, which has been published in final form at https://doi.org/10.1002/ppp.2005. This article may be used for non-commercial purposes in accordance with Wiley Terms and Conditions for Use of Self-Archived Versions.

Reuse
Items deposited in White Rose Research Online are protected by copyright, with all rights reserved unless indicated otherwise. They may be downloaded and/or printed for private study, or other acts as permitted by national copyright laws. The publisher or other rights holders may allow further reproduction and re-use of the full text version. This is indicated by the licence information on the White Rose Research Online record for the item.

Takedown
If you consider content in White Rose Research Online to be in breach of UK law, please notify us by emailing eprints@whiterose.ac.uk including the URL of the record and the reason for the withdrawal request.

UNIVERSITY OF LEEDS
University of Sheffield
UNIVERSITY of York

Relict periglacial soils on Quaternary terraces in the Central Ebro Basin (NE Spain)

Short title: Periglacial soils in the Ebro Basin

R. Rodríguez-Ochoa[1], J.R. Olarieta[1], A. Santana[1], C. Castañeda[2], M. Calle[3], E. Rhodes[4], M. Bartolomé[5], J.L. Peña-Monné[6], C. Sancho[†7]

[1] Departament de Medi Ambient i Ciències del Sòl, Universitat de Lleida, Lleida 25191, Spain. Tlf: 34-973-702612; Fax: 34-973702613; E-mail: rrodriguez@macs.udl.es

[2] Estación Experimental de Aula Dei, EEAD-CSIC, Zaragoza, Spain.

[3] Museo Nacional de Ciencias Naturales, MNCN- CSIC, Madrid, Spain.

[4] Department of Geography, The University of Sheffield, Sheffield, UK.

[5] Instituto Pirenaico de Ecología, IPE-CSIC, Zaragoza, Spain.

[6] Departamento de Geografía y Ordenación del Territorio, Universidad de Zaragoza, Zaragoza, Spain.

[7] Departamento de Ciencias de la Tierra, Universidad de Zaragoza, Zaragoza, Spain.

Authors' accepted version of paper published as Rodríguez-Ochoa R. et al.. Permafrost and Periglacial Processes 2019;1–10. https://doi.org/10.1002/ppp.2005

Abstract

Pedofeatures associated with ancient cold climatic conditions have been recognized in soils on terraces in the Monegros area (central Ebro Basin), at a latitude of 41°49'N and an altitude of 300 m a.s.l. Eleven soil profiles were described on fluvial

deposits corresponding to the most extensive terrace (T5) of the Alcanadre River, Middle Pleistocene in age (MIS8-MIS7). Each soil horizon was sampled for physical, chemical, mineralogical and micromorphological analyses. Macromorphological features related to pedocryogenic processes were described: involutions, jacked stones, shattered stones, detached and vertically oriented carbonatic pendents, fragmented carbonatic crusts, laminar microstructures, succitic fabric, silt cappings on rock fragments and aggregates, and irregular, broken, discontinuous and deformed gravel and sandy pockets. Accumulations of Fe-Mn oxides, dissolution features on the surface of carbonatic stones, and calcitic accumulations were identified related to vadose-phreatic conditions. The observed periglacial features developed under cold environmental conditions in exceptional geomorphic and hydrological conditions. This soil information may have potential implications in studies of the paleoclimate in the Ebro Valley as well as in other Mediterranean areas.

KEYWORDS

Cryogenic pedofeatures, middle latitude, low altitude, calcareous soils, carbonatic accumulations, Monegros

1 INTRODUCTION

Periglacial environments occur in non-glacial high-altitude, high-latitude and continental domains characterized by cold climatic conditions promoting frost-action processes that favour the occurrence of freezing and thawing cycles and/or permafrost[1-3]. In the Iberian Peninsula, periglacial dynamics are currently restricted to the highest mountain areas and very few cases of periglacial features from the Pleistocene have been described in low-altitude inland areas[4-6]. In the Central Ebro Basin (NE Spain), the

17 ka-old stratified scree slopes from Valmadrid are the only periglacial deposits reported in the literature[7]. The deformational features affecting Pleistocene terraces around Zaragoza were interpreted as the result of periglacial cryoturbation and ice wedges by some authors[8-10], but others[4,11-13] proposed gypsum dissolution and diapiric activity as the main drivers of such deformations. Periglacial environments have been associated with 20±3 ka-old loess deposits in the Ebro Basin[14]. Recent works indicate the distribution and remarkable extension of 18-34 ka-old loess deposits related to cold conditions at altitudes of 300-500 m a.s.l. in the lower Ebro Valley[15-16].

The objectives of this work deal with i) the macro and micromorphological characterization of soils and the interpretation of pedocryogenic features identified, and ii) the geomorphic, stratigraphic, and past hydrological, and climatic conditions controlling local periglacial processes in the area.

2 STUDY AREA

The study area is located in the North of Monegros area or Sariñena depression[17], which is drained by the Alcanadre-Flumen River system, and is located within the central sector of the Ebro River Basin (Figure 1)**.** Currently, the Central Ebro valley supports a Mediterranean continental steppe type of habitat. Mean annual temperature in Sariñena village during the 1945-2009 period is 13.7 °C, with January as the coldest month with a mean temperature of 5.3 °C. Mean annual rainfall in the area is 405 mm.

Geological bedrock consists of horizontal layers of sandstones and mudstones of the Sariñena Formation[17] covered by a terrace sequence related to the Alcanadre-Flumen fluvial system composed of nine cut-in-bedrock (strath) and fill Pleistocene terraces[18-19].

3 METHODS

Geomorphological mapping of the Pleistocene terrace sequence of the Alcanadre-Flumen system in the Sariñena high plain was derived from stereoscopic photointerpretation of aerial photographs from 1957 US Air Force flight B, printed at 1:33,000 scale. The resulting geomorphological map was digitized using ArcGIS® 10.3. A digital elevation model generated in 2010 from airborne LiDAR data was used to refine the photointerpretation. A subsequent field survey was carried out across the Sariñena high plain and in the surrounding areas in order to identify different landforms and processes. Fluvial terrace deposits were described using the sedimentary lithofacies codes[20]. We described and sampled 11 pedons (Figure 1) for physico-chemical analyses. Different horizons and carbonatic accumulations were sampled for micromorphology and clay mineralogy analyses in 8 selected pedons.

Soil profiles (Figure S1) were described following[21-22] and classified according to Soil Taxonomy[23]. A total of 122 soil samples were collected for laboratory analyses. Soil samples were air-dried, sieved to 2 mm and analysed for pH (1:2.5 in water), electrical conductivity (1:5 in water), organic carbon (Walkley-Black method[24]), calcium carbonate equivalent (volumetric calcimeter method) and texture (pipette method). The cation exchange capacity was determined as ammonium after saturation with 1 N NH4OAc at pH 7 and extraction with 1 N NaOAc at pH 8.2, and the exchangeable cations (potassium, sodium, magnesium and calcium) by atomic absorption spectrophotometry. Clay mineralogy was studied through X-ray powder diffraction (XRD) using a Bruker D8 Advance diffractometer with graphite-monochromated CuK(a) radiation and a linear Vantec detector. XRD patterns were obtained from random powder mounts and oriented mounts. A total of 64 soil thin

sections (135 × 58, and 58 × 42 mm large) of undisturbed soil horizons and selected soil components were manufactured after impregnation with a cold setting polyester resin and described[25-27].

Three samples were collected for infrared stimulated luminescence dating (IRSL), two of them from the same sand lens in a gravel quarry wall 2 km south of the village of Sariñena (41º46'21''N; 0º10'24''W), and a third sample from another quarry 1 km east of Sariñena (41º47'21''N; 0º8'38''W). Dating was performed using k-feldspar single grain post-IR IRSL procedure[28].

4 RESULTS

4.1 The T5 terrace of the Alcanadre River

The T5 terrace is well preserved along the Alcanadre River valley and, along with the nearby lowest Alcanadre terrace T1[18-19], constitutes a relevant regional landscape marker that facilitates the correlation of other terraces forming the sequence. T5 terrace has a triangular shape with a north-south axis of about 13 km and an east-west axis of 4 km. Landforms related to the Alcanadre River, to the east, and to the Flumen River, to the west, appear on this terrace (Figure 1). The altitude of the tread surface corresponding to the T5 terrace is 30 m above the active channel. The mean slope gradient in this sector is around 4.4 ‰, and the mean thickness of the alluvial cover related to T5 varies between 2.5 and 7 m. Following the Miall terminology, terrace deposits include massive (Gm) and cross-stratified (Gp and Gt) gravels sometimes with basal channel surfaces. Gravels are sub-rounded and well sorted and mostly consist of limestone and sandstone from the Pyrenean External Ranges. Maximum grain size (Dmax) of gravels ranges from 8 to 16 cm and the mean grain size

(D50) from 2 to 5 cm. Interspersed stratified sand (St) lenses and overbank (Fm) silty sediments appear occasionally capping the fluvial fining-upwards sequences.

The remnants of T6 terrace correspond to the residual reliefs of Santa Cruz and Puyalón (Figure 1). Previous work has proposed that this terrace obstructed in the past the external surface drainage and occluded a low-lying zone, thereby creating high water tables that influenced the development of piping processes in the surrounding sodium-rich Miocene clays and the formation of the Sariñena Lake[29] .

Palaeomagnetic data for the T5 terrace indicate a normal polarity and consequently an age younger than the Matuyama-Brunhes reversal at 781 ka BP[18]. The samples analysed by IRSL dating provided ages of 235 ± 17 ka BP, 196 ± 13 ka BP, and 274±18 ka BP. We therefore propose an age ranging from 274 to 222 ka BP for the T5 terrace of the Alcanadre River corresponding to the Marine Isotope Stage MIS8 and the transition to MIS7[30].

4.2 Main soil macromorphology and physico-chemical characteristics

All soils studied showed processes of secondary accumulation of carbonates, frequently producing petrocalcic horizons. On the other hand, only one soil profile showed horizons with clay illuviation (Table S1).

Most soils were well drained, A and B horizons having a prominent reddish colour with a hue from 7.5YR to 5YR, but C horizons frequently showed oxidation-reduction features. Rock fragment content in A horizons was usually smaller than 15%, but it was quite variable in Bwk and Btk horizons, reaching up to 70%, while in Bkm and C horizons it was usually bigger than 70%. The A and Bwk horizons had fine or moderately fine textures while C horizons had moderately coarse or coarse textures. No accumulations or textural features were observed in the A horizons. The Bwk and Btk

149 horizons had frequent nodules, pendents, and coatings of $CaCO_3$, and the latter showed
150 few clay coatings with silt. The Bkm horizons were strongly cemented by carbonates
151 but no textural coatings were observed. C horizons included frequent pendents,
152 coatings, and powdery lime, as well as some coatings of Mn and Fe oxides. Textural
153 coatings of clay with silt also appeared in some coarse C horizons while coatings of silt
154 appeared in some fine C horizons. The synthesis of the soil macromorphological
155 information is reflected in Tables S1 to S4 of the Supporting Information.
156 The soil A and B horizons have moderately alkaline pH and C horizons are
157 strongly alkaline. All horizons are non-saline and calcareous and have low organic
158 matter concentrations. Values of cation exchange capacity are low to moderate,
159 exchangeable sodium percentage is always smaller than 4%, and calcium is the main
160 exchange cation, and therefore conditions are favourable for clay flocculation. Clay
161 mineralogy of the A and B horizons is similar with a great predominance of illites and
162 presence of chlorites. Pyrophyllite and kaolinite appear in a lesser proportion. The
163 synthesis of the physical-chemical and mineralogical information is reflected in the
164 Tables S5 to S8 of the Supporting Information.
165
166 **4.3 Soil cryogenic features**
167 Different cryogenic features have been identified at both the macro- and
168 micromorphological scales: involutions; jacked elements; shattered elements;
169 deformation and fragmentation of soil horizons; lenticular and laminar aggregates;
170 vesicular, vughy and planar porosities; soil cryogenic fabrics and silt cappings.
171 Four types of involution morphologies were identified in the field according to
172 the classification of Vandenberghe[31-32]. We described regularly spaced type 3
173 involutions, in which the lower soil horizons with a high proportion of gravels form

wedges or narrow festoons penetrating the fine or moderately fine textured upper soil horizons, without dividing them. Involutions had a scalloped and symmetrical morphology, and appeared regularly spaced (Figure S2a). In some areas type 2 involutions were observed with spacings and heights of more than 60 cm but without lateral continuity (Figure 2a). Individual type 4 involutions (Figure S2b) and irregular and contorted type 6 involutions (Figure 2b) were also described.

Most non-skeletal soils showed evidence of jacking of clasts up to 18 cm in size (Figures 2b, S2a, S2b), which appeared pointing towards the finer-textured soil horizons above them. Frequently, these verticalized clasts had subsequently developed $CaCO_3$ pendents in the lower side (Figure S5e). Clasts with their pendents rotated close to 90º were commonly found, and in some cases several systems of pendents had developed in the lower part (Figure 2c).

Frost shattering of different types of coherent materials such as alluvial clasts (Figure S2c, S4a, S4b), pendents of $CaCO_3$ (Figures 2d, S3a, S3b, S4c), $CaCO_3$ nodules (Figures 2e, S5a) and carbonatic crusts (Figures S2d, S3c) were identified.

$CaCO_3$ nodules had frequently undergone fracturing and rotation processes followed by the precipitation of an alternating banded filling of spar and micrite/microspar similar to the laminar pendents (Figures 2e, S5e). Such rotation also indicates processes of internal deformation of the horizon by cryoturbation (Figure S5e). Bladed cracks also appeared in laminar pendents (Figure S3b). At the microscopic scale, fractures of textural coatings and redox accumulations of Fe-Mn oxides were also observed (Figure S5b).

Break planes, planar gaps or new porosity often developed along the contact between clasts and their pendents (Figure S5c), or within the calcitic pendents (Figure S5d) or crusts (Figure S3c). These cryogenic features were usually identifiable under

199 the microscope due to the presence of textural coatings and infillings (Figure S3a).
200 Palisade morphologies of spar crystals in some bands of calcite accumulation within the
201 pendents indicated their growth in voids without volume restrictions (Figures S3a, S3b).
202 Features that mainly occurred in non-skeletal horizons included fragmentation
203 and deformation of the limits of C horizons (Figures S2e, S2f), rotation of pendents
204 developed in clasts (Figures 2c, S5e), rotation of nodules with pendents (Figures 2e),
205 and silt cappings made up of two generations (Figure S4d).
206 Frequent lenticular 0.2 -0.4 m thick beddings in fine sandy silt C horizons
207 appeared 2 to 3 m below the terrace surface (Figure 2f). Smooth planar fissures with
208 non-conforming boundaries demarcated the platy aggregates (Figure 2f, S4g). Vesicular
209 porosity was rare (Figure S3d) and vughy was more frecuent (Figure S3d). Vughs,
210 cracks, and triangular or square star-like interpedal connected pores with planar voids
211 (Figure S3e) often occurred in non- skeletal fine-textured C horizons.
212 Rotation and succitic fabrics of sand grains or gravels were described at a
213 microscopic scale in Bwk and Btk horizons (Figure S3f). Areas with an organization
214 with preferential diagonal orientation (Figure S3g), as well as an orbicular rotational
215 fabric with an arched arrangement of the sand grains forming curved bands (Figure S3h)
216 were also identified.
217
218 **4.4 Textural features and Fe-Mn oxide accumulations**
219 Features showing particle translocation, such as coatings, cappings,
220 intercalations, and, in a lesser proportion, infillings and fragments of cutans, were
221 identified in B horizons of some soils. These features were usually complex, i.e. they
222 included several stages or phases of formation that differ in texture and color mainly
223 due to their different grain size. In some cases the coatings had been incorporated into

224 different carbonatic accumulations by the growth of the calcite crystals. These features
225 were distributed within the pedogenic porosity and in cracks of shattered stones (Figure
226 S4c, S4a).

227 Three types of textural pedofeatures were identified based on microscopy
228 birefringence and grain size. One type was composed of impure clay (Figure S4c) and
229 rarely dirty clay, and no clean or micro-laminated clay coatings were detected. A second
230 type was made up of clay mixed with silt in variable proportions (Figures S4a, S4b), silt
231 with some clay, clay with a small proportion of silt, or basal mass. The latter appear in
232 all types of B horizons and in skeletal C horizons (Figure S4e).

233 The third type of textural pedofeature was the occurrence of silt accumulations.
234 They were widespread in non-skeletal C horizons (Figure 2f). In skeletal C horizons
235 these accumulations appeared forming infillings between clasts, link cappings, and
236 cappings (Figure S4f). Pedofeatures with banded fabric (Figure S4g) were also observed
237 in the shape of a complex feature with sandy basal mass with laminar or lenticular
238 microstructure, silt caps, and layers of sorting sands.

239 In some cases, two families of silt cappings were recognized in the same soil
240 horizon representing two mobilization stages of the silty material, a younger capping,
241 linked to soil aggregates and planar porosity, and an older one which appears as near-
242 parallel silty intercalations within the soil groundmass. Figure S3d shows an example of
243 the latter arranged at an angle of about 60º-70º with respect to the direction of the
244 younger caps. Downturned silt cappings caused by soil deformation were also present
245 (Figure S4h).

246 Coatings of Fe and Mn oxides on gravels and coatings made up of fragments of
247 those coatings were described in skeletal C horizons (Figure S2g, S5b), while

impregnative diffuse nodules, hypo-coatings, and intercalations appeared in non-skeletal Bwk, Btk, and C horizons.

4.5 Carbonatic accumulations

The most abundant $CaCO_3$ accumulations were pendents, nodules, and crusts, though pseudomorphs of roots (queras), and infillings with different calcite habits (acicular, microspar, and spar crystals) were also identified. Intense dissolution morphologies were also identified on the surface of carbonatic rock fragments in C horizons with over 70% of coarse fragments (Figure S5h).

Several types of pendents were identified. Laminar pendents, 0.1 to 45 mm thick, appeared at the base of rock fragments (Figures S5c, S5d), carbonatic nodules (Figure 2e), or crusts (Figure 3) in Bwk, Bkm, and Btk horizons. These pendents were organized in coloured alternating bands of grey spar and brown micrite/microspar which suggests alternating clay and fine silt enrichment (Figure S5d). The base of the bands was smooth, wavy, or arched and lacked mammillary or botryoidal structures (Figure S5c, S5d). There were also spar fillings in palisade or double palisade in planar voids (cracks) of cryofractures (Figure S3a, S3b).

Columnar pendents with a length of 4-55 mm and a width of each individual pendent of 0.15-20 mm appeared at the base of laminar pendents of stones and carbonatic crusts (Figures 3, S2h), sometimes coalescing into a stalactitic mammillary to botryoidal appearance (Figures 2g, 2h, S5f), in Bwk horizons and at the base of fractured calcareous crusts. The presence of voids appeared necessary for unrestricted calcite accumulation in these pendents (Figure 3). They were internally organized into alternating arched bands of grey spar and brown micrite/microspar (Figure 2g). The individual spar crystals showed a conspicuous morphology of elongated scalenohedrons

with a prominent radial extinction (Figure S5g). The most frequent form of the lower limit of the bands was scalloped, mammillary, and digitated.

Frequent impregnative $CaCO_3$ nodules were identified in medium to fine textured B horizons. Nodules ranged between 2 and 15 mm in size, were rounded or had vertically elongated sections, and showed varying degrees of purity, the more reddish ones containing a greater proportion of basal mass of the horizon. There were differentiated up to three generations of carbonate accumulations associated with the nodules (Figure S5a), mostly micrite but also microspar, often appearing as pendents. The joint presence of nodule and pendent outside its original position allowed the identification of nodule rotation due to soil deformation processes (Figure 2e). Break planes produced by cryoclastic processes favoured the development of compound accumulations similar to pendents (Figure 2e).

The calcareous crusts were mostly conglomeratic (Figure 2h), but some were nodular-oolithic or with laminar facies at the top. Near-horizontal or cross-plane fractures of the crusts (Figure S2d) with $CaCO_3$ precipitations and coalescent columnar pendents were identified (Figure S2d, S3c).

5 DISCUSSION

5.1 Genesis of pedofeatures

Alternative explanations to the set of features described other than periglacial processes, as proposed by some authors[4], may be rejected. Mass wasting often results in features similar to involutions[33-34], but these processes have not been observed in the soils of the T5 terrace, which has a general slope of about 1%.

Collapses related to karstic processes in gypsum or limestones[11] and volume changes associated with anhydrite expansion into gypsum cannot explain the

298 deformities and fragmentation of soil horizons since the materials underlying the
299 alluvial deposits are detrital rocks, mainly lutite and sandstone, and there are no gypsum
300 rock or limestones in the area. Similarly, expansion-retraction of clay –rich materials
301 may be rejected as no expandable clays have been found in this region[29,35].

302 Windthrow of trees has been shown to cause deformation and involutions in
303 soils[36]. However, the involutions identified in the soils studied are sufficiently
304 generalized spatially, and show a continuity, symmetry and depth that discard this
305 possibility.

306 The hypothesis of collapses due to piping, which is a frequent process in the
307 area[29] can be rejected for similar reasons. Tectonic deformations may also be
308 disregarded as an alternative explanation, even though liquefaction features along the
309 fault line may be mistaken for cryoturbation features[37], because the area presents low
310 seismicity[38-39]. Furthermore, sedimentary structures of load (load cast) or other
311 sedimentary irregularities in the stratification[11] do not seem to correspond to the features
312 described here.

313 Cryoturbation involves processes of sorting, heaving, stirring, wedging, and
314 cracking[2,40]. The occurrence in our soils of all types of involution described by
315 Vandenberghe[31-32], except type 2, requires intense cold conditions, although not
316 necessarily permafrost, and are facilitated by frost-defrost cycles. The traction exerted
317 by the growing of ice lenses within rigid elements (e.g., stones, nodules) included in a
318 matrix susceptible to frost progressively leads to the rotation and vertical alignment of
319 clasts[41-42].

320 The mechanisms involved in frost shattering include frost wedging, ice
321 segregation, and hydraulic fracturing[41]. Frost shattering may also affect pedofeatures,
322 disrupting soft iron nodules, clay coatings, or carbonate precipitates[41]. Deformed and

broken horizons indicate mechanical stresses associated with cryoturbation that results in displacement of the mass, ice segregation, and thermal cracking[40].

Platy structures may be formed by ice segregation and soil desiccation as ice lenses grow in the course of soil freezing[43]. Ice lenses develop perpendicularly to the direction of the freezing front, and thus their orientation is generally parallel to the ground surface. Soil aggregates become somewhat oriented because of repeated freeze-thaw cycles. In frozen state lenticular fabrics are separated by not only horizontal ice lenses but also by diagonal ice veins[44]. The succitic fabric[27] has been identified in differentent B horizons as a result, at microscale, of the traction exerted by growing ice lenses on rigid elements included in a matrix susceptible to frost. This process progressively leads to the rotation and vertical alignment of the clasts[42].

Vesicular porosity results from the expulsion of the air confined by the structural collapse that occurs during thawing, and the subsequent deformation of vesicular pores produces the vughy porosity[43,45].

The clay coatings described cannot be primarily associated with periglacial conditions as they require a temperate climate with moist periods both for the initial formation of clay-sized material and its subsequent mobilization leading to the formation of the coatings[46-47]. Furthermore, the reddish colour of these soils, with a hue of 5YR or 7.5YR that is related to the presence of hematite, suggests a much warmer climate than even the present one[47].

The abundance of textural features, with mixed clay and silt, in the studied soils demonstrates a strong downward migration of fine particles during ground melting[48], and although they are not pure clay cutans in the sense of those described by[25-26], they indicate a certain degree of sorting. These textural features are common in cryogenic soils due to slaking under melting conditions and subsequent vertical frost sorting the

348 sand and coarse silt fractions[40]. These clay and silt textural pedofeatures, as well as the
349 clayey pedofeatures previously discussed, have frequently been incorporated into
350 carbonatic accumulations by the growth of calcite crystals originating Btk and Btkm
351 horizons.

352 Silt cappings are also frequent in C horizons and have been linked to cryogenic
353 processes[46,49]. Silt and sand banded cryogenic fabrics result from a combination of
354 compaction and cryodesiccation between growing ice lenses during soil freezing, and
355 illuviation on the upper surfaces of aggregates during soil thawing[43,50]. Resulting fabrics
356 include dense platy peds separated by planar voids, banded fabrics, and lenticular zones
357 of denser matrix. Many periglacial soils exhibit downward migration of fine particles,
358 notably coarse silt, that bridge sand grains, fill macropores, and occur as caps on coarse
359 fragments[40]. These coatings form due to the melting of the ice lenses and ice coatings
360 around the mineral grains.

361 Coatings of Fe and Mn oxides indicate conditions of soil water saturation and
362 reduction producing Fe^{2+} and Mn^{2+} soluble compounds that are able to migrate in the
363 soil solution and to later reoxidize and precipitate. In some cases cryoturbation
364 processes break up the coatings on clasts and fragments, and the pieces may migrate
365 gravitationally and accumulate in the form of Fe-Mn oxide cappings.

366 The diversity of traits described, their characteristics, and relationships reflect
367 processes of mixing, fracture, displacement and orientation of soil materials which
368 strongly suggest relict periglacial genesis[2,32,40,41,49,51] and underline the complexity of
369 soil-landscape relationships[52].

370

371 **5.2 Carbonatic pedofeatures**

372 Several studies have described cryopedogenic features in soils formed in
373 calcareous parent materials and / or with carbonatic accumulations[53-60].
374 Among all the carbonatic features described in our soils (i.e., pendents, nodules,
375 nodules with pendents, powdery calcite, coatings, acicular crystals, root pseudomorphs,
376 and crusts) only columnar pendents may be associated with pedocryogenic processes,
377 but we do not discard that these processes may have been involved at some stage in the
378 development of some of those carbonatic features.
379 Columnar pendents require space for repeated precipitation of calcite phases.
380 This space may be produced by ice lensing and frost-induced moisture retractions
381 allowing the vertical growth of columnar pendents without space restrictions in a
382 similar pattern to stone jacking[49]. Figure 3 shows particularly well-developed columnar
383 pendents with internal morphology similar to but thicker than those described by[55].
384 Altough the formation of calcareous nodules, laminar pendents, and crusts may
385 not be related to cryoturbation phenomena, their fracturing and the subsequent infilling
386 of cracks with $CaCO_3$, as well as the rotation processes, can be associated with
387 periglaciarism[60]. Many studies demonstrate the role of ice on the mechanical weathering
388 of rocks or other indurated materials[61]. Petrocalcic horizons formed in-between non-
389 indurated soil horizons would be especially prone to cracking and disruption by
390 cryoturbation[60]. The various observations that indicate fragmentation of soil
391 components, translocation of silty and/or clayey materials, and infilling of voids and
392 cracks by precipitation of calcite highlight the complexity and difficulty of elucidating
393 the true temporal sequence of these carbonate pedofeatures for dating purposes as
394 previously noted by[62]. We actually performed U/Th series dating of two petrocalcic
395 horizons sampled from the same quarry as the samples used for IRSL dating but the
396 results were inconsistent between them (113.6±2.5 ka BP and 13.1±2.5 ka BP for the

upper and lower samples, respectively). We suggest that the occurrence of various polycyclic phases within these carbonatic accumulations requires very precise sampling of well-defined and specific features in order to obtain meaningful dating results.

5.3 Palaeoenvironmental significance of periglacial features

The periglacial soil morphologies described are almost limited to the western part of terrace T5 as in the central and eastern zones only some jacking of clasts, prismatic carbonate pendents, and cryoturbation of crusts appeared.

The accumulations of Fe and Mn oxides together with the dissolution features on carbonate clasts in horizons with a high proportion of rock fragments, indicate that the high transmissivity of these horizons may have favoured their contact with a persistent water table with variable temporal saturation in calcite, in support of the hypothesis of a paleohydrological regime with a shallow water table in this area. This hypothesis is coherent with previous work regarding the formation of Sariñena endorheic basin which suggested that the T6 residual reliefs of Santa Cruz and Puyalón (Figure 1) occluded a low-lying zone in the western Sariñena high plain where shallow water was available[29].

Up to now periglacial features at low altitude in the Iberian Peninsula have only been described on the coast of Galicia (northwestern Spain)[63]. Relict periglacial cryoturbations and occasional ice wedge morphologies[4] have been reported in the Duero Basin at a similar latitude to Sariñena but at a higher altitude (about 800 m a.s.l.)[5-6].

The soil morphologies described in Sariñena high plain also suggest conditions of deep seasonal frost. The type 2 involutions are discontinuous and the other periglacial features would require frequent alternating conditions of freezing and thawing and/or long-term and deep seasonal freezing[32]. The thickness of the cryogenic-affected layer, as inferred from the distribution of involutions and frost jacking in the

422 soil profiles, is 1.8 m in average. In Europe, the latitudinal limit of deep seasonal frost
423 for flat areas in France has been suggested at 43º latitude[64-65], though small scale or
424 isolated cryoturbations occur in areas without permafrost that are subject to seasonal
425 frost[40]. We therefore propose deep seasonal frost conditions, and not a continuous
426 periglacial environment, as the main driver of the cryopedogenic features described.
427 To our knowledge, fluvial deposits of terrace T5 and related soils surrounding
428 Sariñena high plane are the only morphopedosedimentary unit affected by periglacial
429 processes in the Quaternary sequence of staircase terraces developed along the
430 Alcanadre River valley. Considering the dates provided by IRSL dating technique the
431 T5 terrace formation occurred from 274 to 222 ka BP, under cold environment with
432 enough water availability to promote the production and transport of sediments to the
433 river channels. The periglacial features studied and associated processes would have
434 taken place at one or more of the various cold periods between 274-222 and 12 ka BP.
435 The aggradation process of terrace T5 was not fed by glaciar outwash pulses
436 because the mountain headwaters (External Pyrenean Range) were not glaciated during
437 the Quaternary. Alternatively, it would be related to periglacial environmental
438 conditions[66] with enough water availability to enhance the sediment supply. Moreover,
439 the sparse steppe vegetation and the seasonal distribution of rainfall might have
440 favoured runoff from slopes and intensified mechanical bedrock weathering[67].
441 Therefore, we suggest the prevalence of periglacial conditions in the source areas
442 feeding the sedimentary fluvial aggradation in the Alcanadre River valley around 274-
443 222 ka BP. During the subsequent soil formation phase water availability would have
444 decreased ceasing the alluvial activity while cold conditions would remain favouring
445 active periglacial processes in soils and sediments.
446

6. CONCLUSIONS

Relict periglacial features have been identified in calcareous soils of a fluvial terrace at a middle latitude (41º49'N) and a low altitude of 300 m a.s.l. in Europe. The soil horizons showed a variety of cryopedogenic features at different scales, from the field to the microscope, which are related to the deformation and disruption of soil components and translocation of material due to deep seasonal frost conditions. These macro and microfeatures, which are unique in the region, are the result of specific edaphic conditions related to the occurrence of a shallow water table under a cold dry seasonal-frost climate and soil materials with different frost susceptibility. The periglacial features studied would have developed between 274-222 and 12 ka BP.

The presence of cryopedogenic features in soils of the Middle Ebro Valley may have significant implications regarding the use of these and other mid-latitude calcareous soils for geochronology and palaeoenvironmental reconstruction.

The calcareous composition of soils has conditioned the formation of conspicuous microfeatures. A possible cryogenic genesis for columnar carbonate pendents is proposed. Further work on the specific cryogenic processes associated with features in calcic horizons is required, as well as a more precise dating of these features.

ACKNOWLEDGEMENTS

This study was funded by the Spanish Ministry of Economy, Industry and Competivity under the projects CGL 2017-89603-R and PCI2018-092999. We thank Ramón Juliá (ICTJA-CSIC), Ignacio Bilbao and Natividad Segura for their field support and helpful discussions, and César Trillo for the facilities provided. We are grateful to the three anonymous reviewers for their helpful comments on a previous version.

472 We dedicate this paper to the memory of our colleague Carlos Sancho, who
473 passed away while this paper was under review.
474
475 **SUPPORTING INFORMATION**
476 **Figure S1** Cryogenic macromorphological features
477 **Figure S2** Cryogenic micromorphological features
478 **Figure S3** Cryogenic micromorphological textural features
479 **Figure S4** Micromorphological carbonatic and redox features
480 **Table S1** Macromorphological characteristics of the studied soils
481 **Table S2** Macromorphological features of pedon SAR-10
482 **Table S3** Macromorphological features of pedon SAR-11
483 **Table S4** Macromorphological features of pedon SAR-12
484 **Table S5** Physical and chemical data of pedon SAR-10
485 **Table S6** Physical and chemical data of pedon SAR-11
486 **Table S7** Physical and chemical data of pedon SAR-12
487 **Table S8** Clay mineralogy of selected soil horizons
488
489 **REFERENCES**

490 1. Tricart J, Cailleux A. *Le Modelé des Régions Périglaciaires. Traité de*
491 *Géomorphologie, tome II,* Paris: SEDES. 1967.
492 2. Washburn AL. 1980. *Geocryology*. New York: Wiley. 1980.
493 3. French HM. *The Periglacial Environment*, *Third Edition*. Wiley: Chichester.
494 2007.

4. Gonzalez-Martín JA, Pellicer F. Rasgos generales del periglaciarismo de la península Ibérica: Dominio continental de las tierras del interior. *Cuad Inv Geogr.* 1988; 14: 23-80.
5. Serrano E, Pelleteiro R, Otero M. Huellas pleistocenas de frío intenso en la Cuenca del Duero: Cuñas de arena relícticas en las terrazas del Pisuerga. In: Úbeda X, Vericat D, Batalla RJ, eds. *Avances de la Geomorfología en España*, 2008-2010. Barcelona: SEG-Universitat de Barcelona; 2010: 417-420.
6. Oliva ME, Serrano A, Gomez-Ortiz MJ et al. Spatial and temporal variability of periglaciation of the Iberian Peninsula. *Quat. Sci. Rev.* 2016; 137: 176-199
7. Valero-Garcés B, González-Sampériz P, Navas A, et al. Paleohydrological fluctuations and steppe vegetation during the last glacial maximum in the central Ebro valley (NE Spain). *Quat Int*. 2004; 122, 43-55
8. Brosche KU. Neue beobachtugen zu vorzeitlichen periglazialerscheinungen im Ebrobecken. *Z Geomorph N.F*. 1971; 15:107-114.
9. Brosche KU. Vorzeitliche periglazialerscheinungen im Ebrobecken in der ungebung von Zaragoza sowe ein beitrag zur ausdehnung von schuttund bloakdecken in zentral-und-w-teil der Iberische habinsel. *Gotting Geogr Abh.,* 1972; 60: 293-316.
10. Johnson G. Cryoturbation at Zaragoza, Northern Spain. *Z Geomorph N.F.*1960; 4:74-80.
11. Van Zuidam R. 1976. Periglacial-like features in the Zaragoza region (Spain*). Z Geomorph N.F*. 1976; 20:227-234.
12. Bomer B. Les phenomenes periglaciares dans le Bassin de l'Ébre et ses marges (Espagne).In: Colloq. *Perigl. d'altitude du domaine Mediterranéen et abords.* Strasburg 12-14 mai 1977. Assoc Geogr. D'Alsace, pp 169-176.

13. Simón JL, Soriano A. Diapiric deformations in the Quaternary deposits of the central Ebro Basin, Spain. *Geol. Mag.* 1986; 123: 45-57.
14. Lewis C, McDonald E, Sancho C, Peña-Monne JL, Rhodes E. Climatic implications of correlated Upper Pleistocene glacial and fluvial deposits on the Cinca and Gállego Rivers (NE Spain) based on OSL dating and soil stratigraphy. *Global Planet Change.* 2009; 67: 141-152.
15. Boixadera J, Poch RM, Lowick SE, Balasch JC. Loess and soils in the eastern Ebro Basin. *Quat Int.* 2015; 376: 114-133.
16. Rodríguez-Ochoa R., Balasch JC, Olarieta JR et al. Loess deposits in the lower Ebro Basin (NE Iberian Peninsula). In: Simó I, Poch RM, Pla I, eds. *Proceedings of the 1st World Conference on Soil and Water Conservation under Global Change-CONSOWA*. Lleida: Universitat de Lleida; 2015: 103-106.
17. Quirantes J. *Estudio Sedimentológico y Estratigráfico del Terciario Continental de los Monegros.* Zaragoza: Instituto Fernando el Católico (CSIC); 1978.
18. Calle M, Sancho C, Peña JL, Cunha P, Oliva-Urcia B, Pueyo E. La secuencia de terrazas cuaternarias del río Alcanadre (provincia de Huesca): Caracterización y consideraciones paleoambientales. *Cuad Inv Geogr.* 2013; 39: 159-178.
19. Sancho C, Calle M, Peña-Monné JL et al. Dating the Earliest Pleistocene alluvial terrace of the Alcanadre River (Ebro Basin, NE Spain): Insights into the landscape evolution and involved processes. *Quat. Int.* 2016; 407: 86-95.
20. Miall AD. Lithofacies types and vertical profile models in braided river deposits: a summary. In: Miall AD, ed. Fluvial Sedimentology. *Can. Soc. Pet. Geol. Mem.* 1977; 5: 597-604.
21. Schoeneberger PJ, Wysocki DA, Benham EC. *Field Book for Describing and Sampling Soils. V. 3.0.* Lincoln, USA: National Soil Survey Center; 2012.

545 22. CBDSA (Comisión del Banco de Datos de Suelos y Aguas). *SINEDARES. Manual para la Descripción Codificada de Suelos en el Campo*. Madrid:
546 Ministerio de Agricultura, Pesca y Alimentación; 1983.
547 23. Soil Survey Staff. *Keys to Soil Taxonomy, 12th ed*. Washington: US Department
548 of Agriculture; 2014.
549 24. Walkley, A, Black IA. An examination of the Degtjareff method for determining
550 soil organic matter, and a proposed modification of the chromic acid tritation
551 method. *Soil Sci*. 1934; 37: 29-38.
552 25. Bullock P, Fedoroff N, Jongerius A, Stoops G, Tursina T. *Handbook for Soil*
553 *Thin Section Description.* Wolverhampton: Waine Research Publ. 1985.
554 26. Stoops G. *Guidelines for Analysis and Description of Soil and Regolith Thin*
555 *Sections.* Madison, Wisconsin: Soil. Sci. Soc. Amer. Inc.; 2003.
556 27. Fox CA, Protz R. Definition of fabric distributions to characterize the
557 arrangement of soil particles in the Turbic Cryosols. *Can J Soil Sci.* 1981; 61:
558 29-34.
559 28. Rhodes EJ. Dating sediments using potassium feldspar single-grain IRSL: Initial
560 methodological considerations. *Quat Int.* 2015; 362: 14-22.
561 29. Castañeda C, Gracia FJ, Rodríguez-Ochoa R et al. Origin and evolution of
562 Sariñena Lake (central Ebro Basin): A piping-based model. *Geomorphology*
563 2017; 290: 164-183.
564 30. Lisiecki, LE, Raymo, ME. A Pliocene-Pleistocene stack of 57 globally
565 distributed benthic δ18O records. *Paleoceanogr.* 2005; 20: PA 1003.
566 31. Vandenberghe J. Cryoturbations. In: Clark MJ, ed. *Advances in Periglacial*
567 *Geomorphology*. New York: Wiley; 1988: 179–198.

569 32. Vandenberghe J. Cryoturbation structures. In: Elias SA, ed. *The Encyclopedia of*
570 *Quaternary Science*, vol. 3. Amsterdam: Elsevier; 2013: 430-435.
571 33. Harris C. Mechanisms of mass movement in periglacial environments. In:
572 Anderson M, Richard K, eds. *Slope Stability.* London: Wiley; 1986: 531-559.
573 34. Van Vliet-Lanoë B. The significance of cryoturbation phenomena in
574 environmental recontruction. *J Quat. Sci.* 1988; 3(1): 85-96.
575 35. Rodríguez-Ochoa R, Usón A, Olarieta JR, Herrero J, Porta J. Irrigation from the
576 sixties: Flumen-Monegros. In: Boixadera J, Poch RM, Herrero C, eds, *Tour*
577 *Guide 8B: Soil Information for Sustainable Development.* Lleida: International
578 Union of Soil Sciences; 1998: 1-51.
579 36. Armson KA, Fessenden RJ. Forest windthrows and their influence on soil
580 morphology. *Soil Sci Soc Amer Proc.* 1973; 37 (5): 781-783
581 37. Borchardt G, Taylor G, Rice S. *Fault Features in Soils of the Mehrton*
582 *Formation, Auburn Damsite, California.* Sacramento: California Division of
583 Mines and Geology; 1980.
584 38. Arlegui LE, Simón JL. Fracturación y campos de esfuerzos en el Cuaternario del
585 sector central de la Cuenca del Ebro. *Rev Cuat Geomorf.* 2000; 14(1-2): 11-20.
586 39. Peláez Montilla JA, López Casado C. Seismic hazard estimate at the Iberian
587 Peninsula. *Pure Appl Geophys.* 2002; 159: 2699–2713.
588 40. Bockheim JG, Tarnocai C. Recognition of cryoturbation for classifying
589 permafrost-affected soils. *Geoderma,* 1998; 81 (3–4): 281-293.
590 41. Van Vliet-Lanoë B, Fox C, Gubin. Micromorphology of Cryosols. In: Kimble
591 JM, ed. *Cryosols: Permafrost Affected Soils.* Berlin: Springer; 2004: 365-390.

592 42. Van Vliet-Lanoë B. Patterned ground and climate change. In: Podrovsky O, ed,
593 *Permafrost: Distribution, Composition and Impacts on Infrastructure and*
594 *Ecosystems.* New York: Nova Science Publishers; 2014: 67-106
595 43. Van Vliet-Lanoë B. Frost effect in soils. In: Boardman J, ed. *Soils and*
596 *Quaternary Landscape Evolution*. London: Wiley; 1985: 117-158.
597 44. Ping CL, Michaelson GJ, Kimble JM et al. Cryogenesis and soil formation along
598 a bioclimate gradient in Arctic North America. *J Geophys Res.* 2008; 113:
599 G03S12.
600 45. Van Vliet-Lanoë B, Coutard JP, Pissart A. Structures caused by repeated
601 freezing and thawing in various loamy sediments. A comparison of active, fossil
602 and experimental data. *Earth Surf Proc Land.* 1984; 9:553-565.
603 46. Tarnocai C, Smith CAS. Micromorphology and development of some central
604 Yukon paleosols, Canada. *Geoderma*, 1989. 45: 145-162.
605 47. Dampier L, Sanborn P, Smith S, Bond J, Clague JJ. Genesis of upland soils,
606 Lewes Plateau, central Yukon. Part 2: Soils formed in weathered granitic
607 bedrock. *Can J Soil Sci*. 2011; 91: 579-594.
608 48. Dimase AC. Fossil cryogenic features in paleosols of southern Italy:
609 Characteristics and paleoclimatic significance. *Quat Int.* 2006; 156/157:32–48
610 49. Van Vliet-Lanoë B. Frost action. In Stoops G, Marcelino V, Mees F., eds,
611 *Interpretation of Micromorphological Features of Soils and Regoliths.*
612 Amsterdam: Elsevier; 2010: 81-108.
613 50. Van Vliet-Lanoë B. The significance of cryoturbation phenomena in
614 environmental recontruction. *J Quat Sci.* 1988; 3 (1): 85-96.
615 51. Vandenberghe J, Renssen H, Roche DM et al. Eurasian permafrost instability
616 constrained by reduced sea-ice cover. *Quat Sci Rev.* 2012; 34:16–23.

52. Dillon JS. *Soils and Soil-Forming Processes in a Cool-Dry Environment: the Upper Green River Basin, W.Wyoming U.S.A.* [PhD dissertation]. Lawrence, Kansas: University of Kansas; 2002.

53. Mermut AR, St. Arnaud RJ. A micromorphological study of calcareous horizons in Saskachewan soils. *Can J Soil Sci.* 1981; 61:243-260.

54. Dijkmans JWA, Koster EA, Galloway JP and Mook WG Characteristics and origin of calcretes in a subartic environment, Great Kobuk Sand Dunes, northwestern Alaska, USA. *Arctic Alpine Res.* 1986; 18: 1443-1452.

55. Blank RR, Fosberg MA. Micromorphology and classification of secondary calcium carbonate accumulations that surround or occur on the undersides of coarse fragments in Idaho (USA). In: Douglas LA, ed, *Soil Micromorphology: A Basic and Applied Science*. Amsterdam: Elsevier; 1990: 341-347.

56. Karlstrom ET. Relict periglacial features east of Waterton-Glacier parks, Alberta and Montana, and their paleoclimatic significance. *Permafr Periglac Process.* 1990; 1: 221-234.

57. Van Vliet-Lanoë B, Dumont JL, Verrecchia E. Précipitations cryogeniques de carbonates de calcium: mithe ou réalité. In: Lecolle F, ed*, Les Tufs et Travertins Quaternaires des Bassins de la Seine et de la Somme, et des Régions Limitrophes*. Caen: Centre Géomorphol. Bull. 1990; 38: 55-66.

58. Courty MA, Marlin C, Dever L, Tremblay P, Vachier P. The properties, genesis and environmental significance of calcitic pendents from the High Arctic (Spitsbergen). *Geoderma,* 1994; 61: 71-102.

59. Vogt T, Corte AE. Secondary precipitates in Pleistocene and present cryogenic environments (Mendoza Precordillera, Argentina, Transbaikalia, Siberia, and Seymur Island, Antarctica). *Sediment*. 1996; 43: 53-64.

60. Dillon JS, Sorenson CJ. Relict cryopedogenic features in soils with secondary carbonate horizons, W.Wyoming, USA. *Permafr Periglac Process.* 2007;18(3): 285-299.
61. Murton JB, Coutard JP, Lautridou JP, Ozouf JC, Robinson DA, Williams RBG. Physical modeling of bedrock brecciation by ice segregation in permafrost. *Permafr Periglac Process.* 2001; 12: 1127-1129.
62. Brock AL, Buck BJ. A new formation process for calcic pendants from Pahranagat Valley, Nevada, USA, and implication for dating Quaternary landforms. *Quat Res.* 2005; 63: 359– 367.
63. Blanco Chao R, Costa Casais M, Martínez Cortizas A, Pérez Alberti A, Trenhaile AS. Evolution and inheritance of a rock coast: western Galicia, northwestern Spain. *Earth Surf Proc Land.* 2003; 28(7): 757-775.
64. Andrieux E, Bertran P, Saito K. Spatial analysis of the French Pleistocene permafrost by a GIS database. *Permafr Periglac Process.* 2015; 27(1): 17-30.
65. Bertran P, Andrieux E, Antoine P, et al. Distribution and chronology of Pleistocene permafrost features in France: database and first results. *Boreas,* 2014; 43: 699–711.
66. Chorley RJ, Schumm SA, Sugden DE. 1984. *Geomorphology*. London: Methuen; 1984.
67. Fuller I, Macklin M, Lewin J, Passmore D, Wintle A. River response to high frequency climate oscillations in southern Europe over the past 200 ky. *Geology,* 1998; 26: 275-278

668 Figure captions

669

670 FIGURE 1. Geomorphological map and soil location on Quaternary terraces in
671 the Central Ebro Basin (NE Spain).

672

673 FIGURE 2. Macro- and micromorphological cryogenic features. (a): Type 2
674 involutions. Soil SAR-18. (b) Type 6 contorted Involutions. Soil SAR-15. (c):
675 Calcitic laminar pendent rotated three times (successive vertical axes are
676 indicated by the white arrows). Soil SAR13/1, Bwk. Image PPL. (d): Carbonatic
677 laminar pendent fragmented and jacking, soil SAR-13/2 Ck1. Image PPX. (e):
678 Fragmented and rotated (arrow indicates the pendent vertical axis) calcareous
679 nodule (n) with pendents (p). Soil SAR-12, Bwk2. Image PPL. (f): Silt capping
680 (arrows) and laminar microstructure. SAR13/2 Ck. Image PPL. (g): Columnar
681 pendent with banded organization. Soil SAR-7, Bkm. Image PPX. (h):
682 Carbonatic crust with columnar pendent. Soil SAR-7, Bkm.

683

684 FIGURE 3. Columnar pendent formed under a carbonatic crust. Soil SAR-7
685 Bkm horizon. (a): Scanned soil thin section. (b): Illustrated thin section
686 highlighting different growing steps. A: Carbonate crust with reddish (r) and
687 grey (g) zones; B: Laminar pendent including Bkm fragments (f); C: Columnar
688 pendent with Bkm fragments (f) at the apices of the columns structure; D:
689 Groundmass infillings.

690

691

692

693 Figure 1

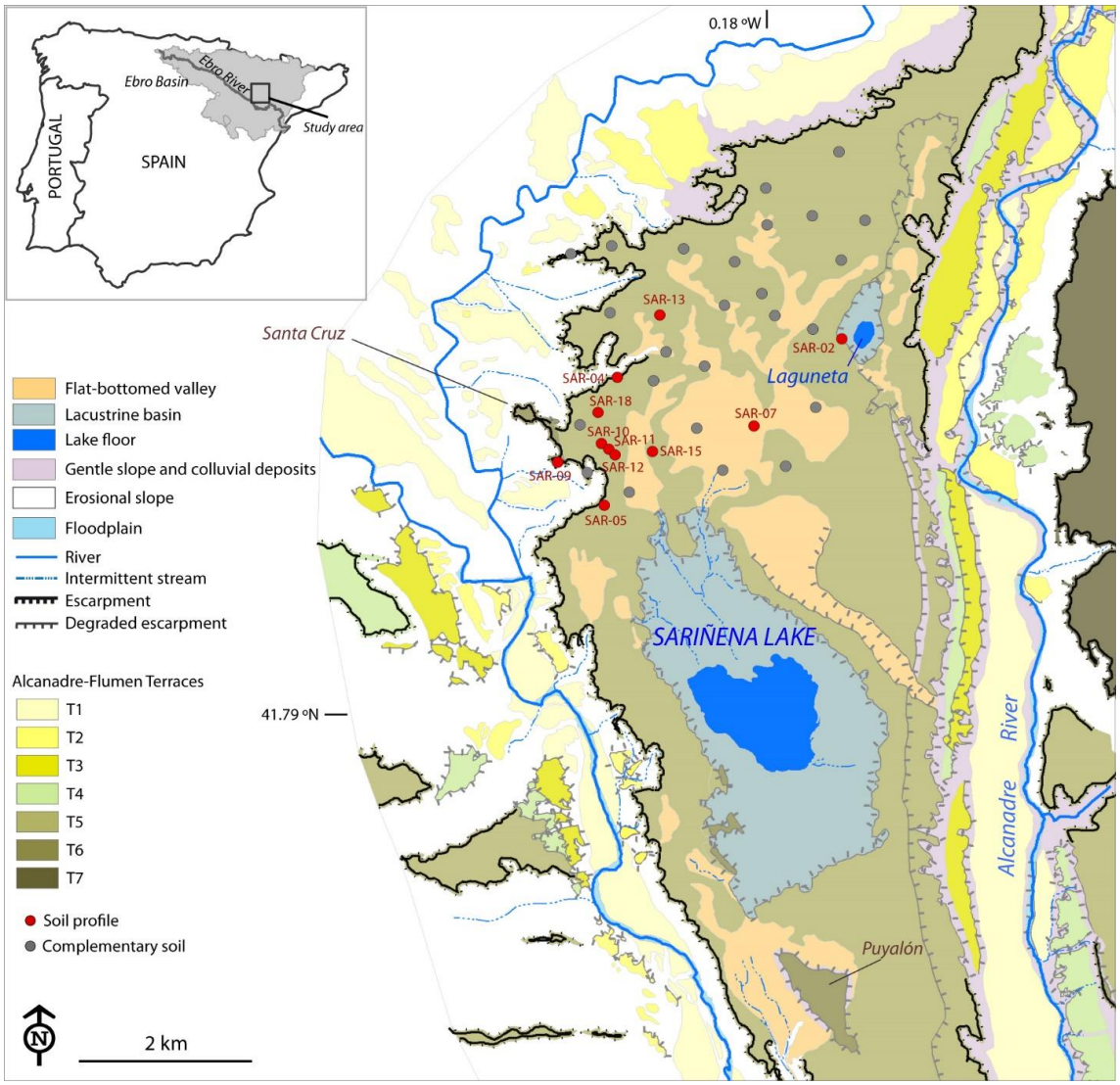

694

695

696

697

698 Figure 2

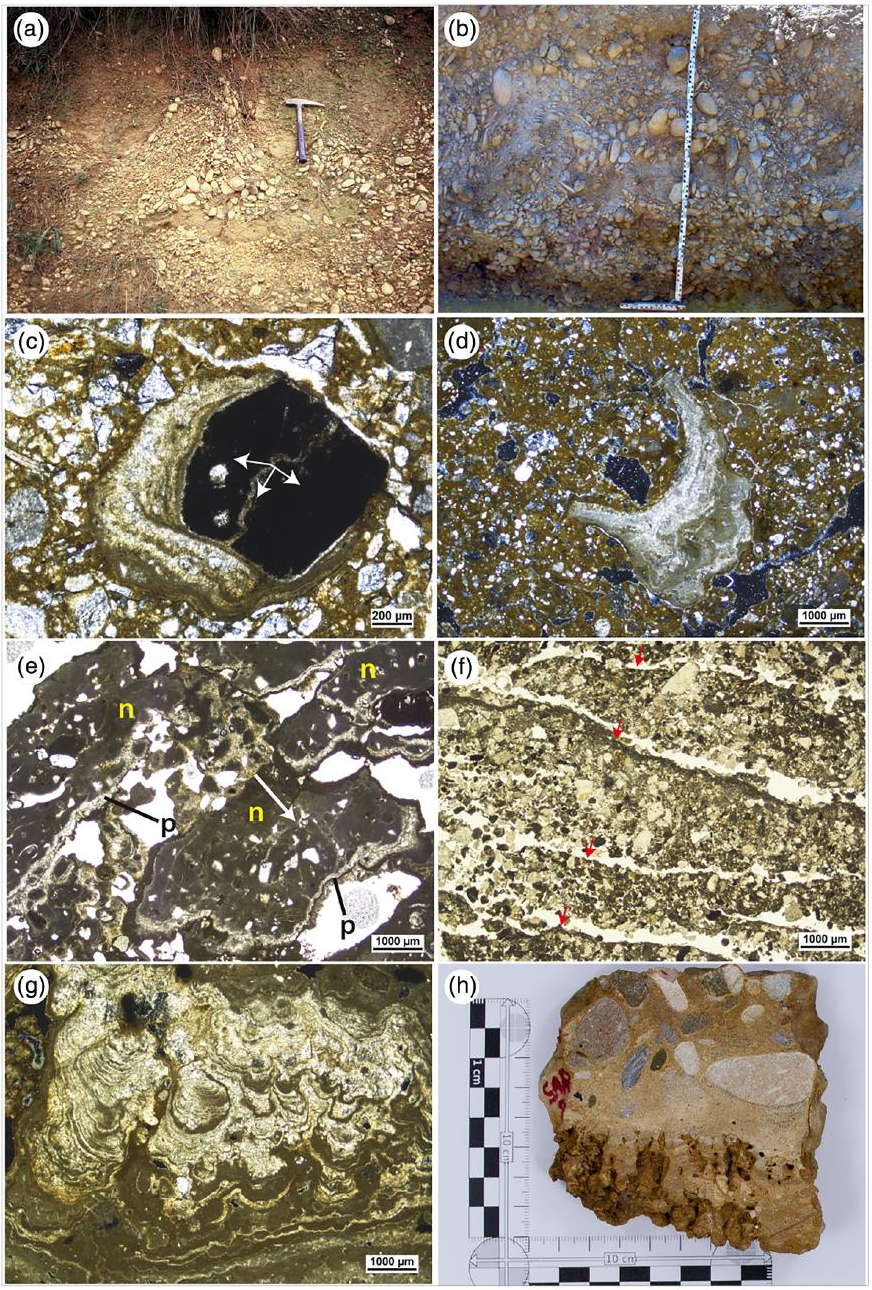

699

700

701

702

703

704
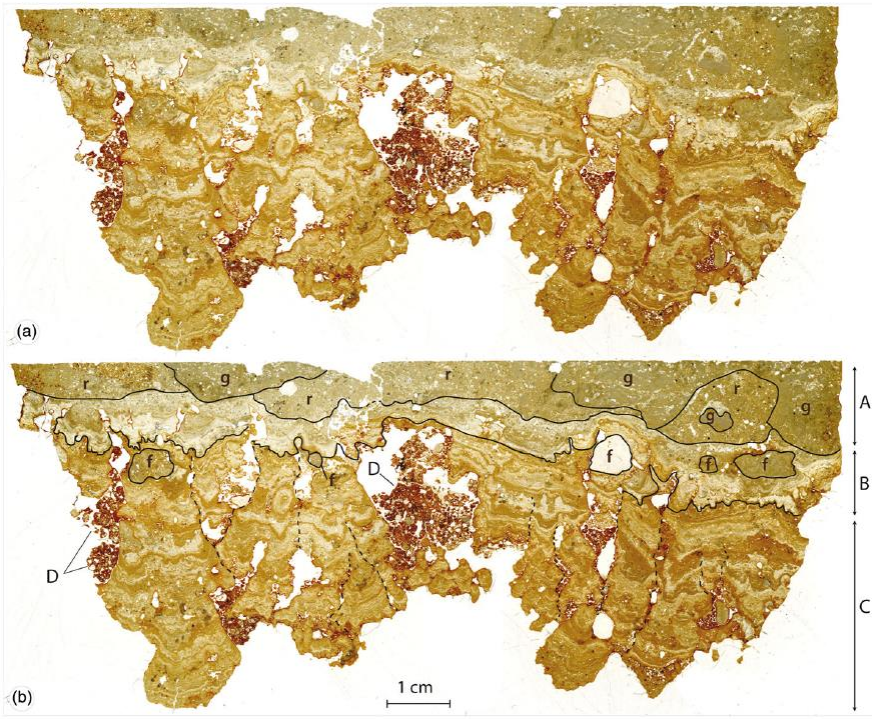
705 Figure 3